Journal of Physics:
Conference Series

PURPOSE-LED
PUBLISHING™

PAPER • OPEN ACCESS

Implementation of different techniques for removing artifacts in diaphragmatic SEMG, and evaluation of these in automatic and online applications

To cite this article: D A Valle and A M Hernández 2021 *J. Phys.: Conf. Ser.* **1921** 012003

View the article online for updates and enhancements.

You may also like

- Surface muscle pressure as a measure of active and passive behavior of muscles during gait
Don A. Yungher, Michael T. Wininger, J.B. Barr et al.
- HD-sEMG-based research on activation heterogeneity of skeletal muscles and the joint force estimation during elbow flexion
Cong Zhang, Xiang Chen, Shuai Cao et al.
- Toward direct biocontrol using surface EMG signals: Control of finger and wrist joint models
Narender P. Reddy and Vineet Gupta

This content was downloaded from IP address 191.95.147.236 on 02/02/2026 at 01:20

Implementation of different techniques for removing artifacts in diaphragmatic sEMG, and evaluation of these in automatic and online applications

D A Valle and A M Hernández

Bioinstrumentation and Clinical Engineering Research Group - GIBIC, Bioengineering Department, Engineering Faculty, Universidad de Antioquia UdeA, Calle 70 No. 52-21, Medellín, Colombia

E-mail: *andres.valle@udea.edu.co*

Abstract: Respiratory muscles superficial electromyography (sEMG) is an important source of information in the monitoring of ventilated patients. One of the main problems in the acquisition of sEMG signals is the different sources of interference. The most common artifacts are the baseline wander (BW) normally generated by motion, and power line interference (PLI). In this paper, different methods were selected and evaluated for the removal of these artifacts in a simulated sEMG signal of the right diaphragm muscle. The best performance technique for the removal of each artifact was determined using frequency analysis and estimation of criteria such as the signal to noise ratio, relative error, cross-correlation, and coherence of the power spectrum density. The computational cost of each of the techniques was estimated to also assess how appropriate it is to implement in online applications and limited hardware. The study demonstrates that the spectral interpolation technique has a good performance in removing PLI from the sEMG signal but has a high computational cost, unlike the adaptive LMS filter. On the other hand, the SSA-based technique proved to be the best performing for BW removal and its computational cost is adequate in a more limited hardware system.

Keywords: *Diaphragm sEMG, Baseline wander, Power line interference, Digital signal processing, EMD, SSA, Adaptive filter*

1. INTRODUCTION

During the last decades, the sEMG has been positioned as a very useful tool, not only in the academic field but also in the medical field, since the information it provides sheds light on the physiological and pathophysiological behavior of muscle function [1,2]. Therefore, the sEMG corresponding to the respiratory muscles can be of great diagnostic help and constant monitoring of patients in medical environments [1,3]. Its usefulness has been demonstrated also in the case of critical mechanically ventilated patients [4].

The analysis of the sEMG signals of respiratory muscles to support the diagnosis requires a signal without noise and ideally without interference because it is about deep muscles in which biopotentials in critical conditions are highly affected by thoracic edema, fat or the inherent muscle fatigue [5,6]Among the most common interferences that affect the sEMG signals are the power line (PLI) [6–10], the baseline wandering (BW) [5,6,11–13]that is normally generated by motion artifacts [4,10], biopotentials interference related to the heart activity[14,15], and interference of non-respiratory

Content from this work may be used under the terms of the Creative Commons Attribution 3.0 licence. Any further distribution of this work must maintain attribution to the author(s) and the title of the work, journal citation and DOI.
Published under licence by IOP Publishing Ltd

muscles (crosstalk)[16,17].The acquisition of the sEMG in clinical implementations or that require online processing and with automatic removal techniques makes noise contamination an even more challenging problem [18–20].

Conventional linear digital filters are not recommended for the removal or reduction of artifacts in sEMG because attenuate the sEMG where there is a spectral overlap between the noise and the signal [6]. Therefore, one of the main challenges is the removal of artifacts without distorting the sEMG signal [6,11]. Another great challenge is the performance of removal techniques in online and automatic applications as the monitoring of the work of breathing and breathing rate of a ventilated patient [6]. Another application in non-respiratory muscles would be for prosthesis control, muscle dysfunction diagnosis, among other types of applications [11–13].The artifact removal techniques for sEMG signals can be separated into two large fields, on the one hand, the removal of artifacts common to all biopotentials, which are not of physiological origin, and another field that depends on each application and the type of muscle involved. Regarding the techniques focused on the removal of artifacts that are not of physiological origin, which are the purpose of this article, different techniques have been proposed and they mainly focus on two types of interference, Baseline Wander (BW) generated by motion artifacts, perspiration and poor electrode contact [21] and Power Line Interference (PLI).

For the removal of PLI the following techniques have been proposed: an adaptive LMS filter [9], a spectrum interpolation technique [8,10], and an empirical mode decomposition (EMD) based technique [6]. For the removal of BW artifacts, the following techniques have been proposed: a high-pass filter [5], an EMD-based technique [6], and a singular spectrum analysis (SSA) based technique [22]. In this study, these techniques were applied in a model of an artifactual sEMG signal of the diaphragm, it was implemented both in a sEMG signal non affected by ECG interference and in a signal affected by ECG interference. The results were compared through a frequency analysis between the simulated sEMG signal with the signals obtained using the techniques and the criteria of signal-to-noise ratio, relative error, and cross-correlation. At last, the performance of each of the techniques in an online implementation is evaluated, the computational cost of each of the techniques and the delay is determined.

2. METHODS

Because this study uses simulated signals, the methodology includes three sections. First, the models used to generate electromyographic and electrocardiographic signals as well as the interferences are described; later the filtering techniques to be evaluated are described, and finally, the performance evaluation strategy is detailed.

2.1. Modeled interfered sEMG signals

To evaluate the artifact reduction techniques, knowledge of the characteristics of the clean signal is required to calculate the residual interference after the application of the different filtering methods, which is why simulation of the sEMG signal is necessary. Also, an ECG signal is simulated, which is summed to the sEMG signal, since the recording of sEMG in the diaphragm normally has ECG artifacts present, the performance of the artifact reduction techniques are evaluated using sEMG with ECG interference and without it.

2.1.1 The sEMG signal

the model consists of two steps: 1) a white zero-mean Gaussian noise source $g(t)$ and, 2) the implementation of a linear filter with a transfer function H, that introduces the spectral characteristics for each of the respiratory phases, inspiration or expiration [14]. The variance of each of the phases of the respiratory cycle, as well as the transfer functions, are estimated from a real sEMG signal[23].

The variances that were estimated for both the expiration and inspiration phases were $8.14x10^{-5}$ and

$2.92x10^{-4}$ respectively, the transfer function for the AR filters used has order 4. The outputs of each filter were modulated by (1).

$$ms(t) = \sqrt{\frac{b_1}{1+\lambda_0}\left[\lambda_0 + sin\left(\frac{2\pi t}{T_p} + \phi\right)\right]^+ + b_2} \quad (1)$$

When $\lambda_0 > 0$, $b_1 > 0$, $b_2 \geq 0$, and the phase angle is ϕ. T_p is the time of a respiration cycle and the operator $[x]^+$indicates that is equal to x when $x > 0$, and is equal to 0 when $x \leq 0$[23,24]. In the sEMG, the time of the respiratory cycle has small variations, therefore T_p has a variation in time. Therefore, it is multiplied by a scalar, where the scalar value is a number randomly taken from the range [0.9,1.1], as can be seen in (2).

$$T_p = \alpha T_0 \quad (2)$$

The maximum value of (1) is the following:

$$ms_{max} = \sqrt{b_1 + b_2} \quad (3)$$

Finally, the function for inspiration is as see in (4).

$$ms_i(t) = \frac{ms(t)}{ms_{max}} \quad (4)$$

And for expiration is the following expression:

$$ms_e = 1 - ms_i(t) = 1 - \frac{ms(t)}{ms_{max}} \quad (5)$$

The values of the variables of the previous equations were taken from previous studies($b_1 = 1$, $b_2 = 0$, $\lambda_0 = 0.5$, $\phi = -\frac{\pi}{6}$, and $T_0 = 4s$)[23,24]. The sEMG signal for the simulated diaphragm is seen in Figure 1(a).

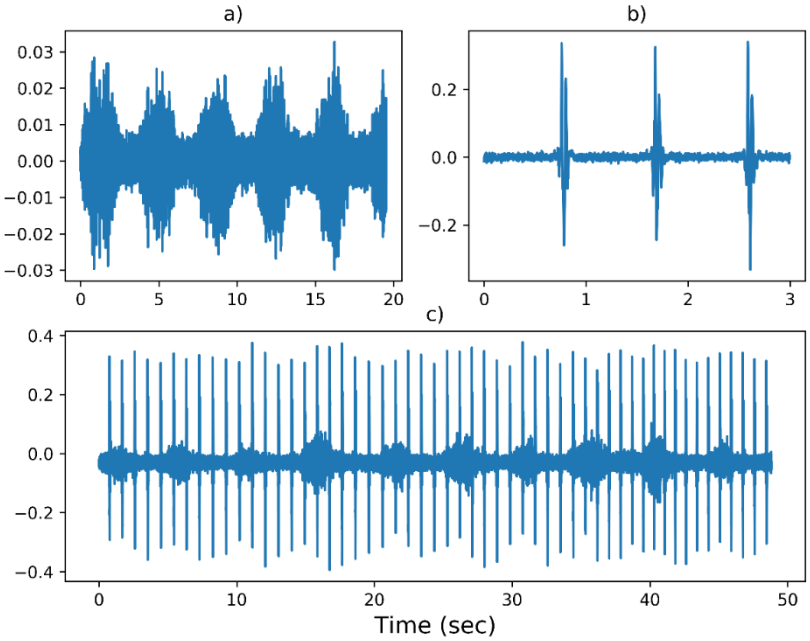

Figure 1. Result of the models. a) simulated sEMG generated from the model; b) simulated ECG generated from the model; c) sEMG simulated contaminated with ECG

The ECG was simulated using a dynamic model based on three ordinary differential equations[25].

$$\dot{x} = \alpha x + \omega y \tag{6}$$

$$\dot{y} = \alpha y + \omega x \tag{7}$$

$$\dot{z} = \sum_{i\epsilon\{P,Q,R,S,T\}} \alpha_i \Delta\theta_i \exp\left(-\frac{\Delta\theta_i^2}{2b_i^2}\right) - (z - z_0) \tag{8}$$

Where $\alpha = 1 - \sqrt{x^2 + y^2}$, $\Delta\theta_i = (\theta - \theta_i) mod(2\pi)$ *and* $\theta = atan2(y, x)$. With $-\pi \leq atan2(y, x) \leq \pi$, ω is the angular velocity of the trajectory as it moves around the limit cycle and also, z_0 is the baseline wander by summing the value with the respiratory frequency f_2 as is shown in (9)[25].

$$z_0 = A\sin(2\pi f_2 t) \tag{9}$$

Where $A = 0.15mV$. Using the dynamic model, the RR intervals of the ECG signal are generated, which corresponds to one turn of the limit cycle. By varying the angular velocity, the length of each RR interval is varied[25].

A bimodal power spectrum $S(f)$, which consists of the sum of two Gaussian distributions is added to the RR interval. Which simulates the effect of the RSA and Mayer waves on the power spectrum of the RR-intervals[26,27].

Estimating the inverse Fourier transform of a sequence of complex numbers and phase amplitudes that can be randomly distributed among 0 and 2π, the interval RR with spectral power of $S(f)$can be obtained[25]. By multiplying a suitable scalar and summing a compensation value, the standard deviation and means required for the RR interval can be provided[25,27]. Finally, the angular velocity of time-dependent motion around the limit cycle, the equation is given by (10).

$$S(f) = \frac{\sigma_1^2}{\sqrt{2\pi c_1^2}} \exp\left(\frac{(f - f_1)^2}{2c_1^2}\right) + \frac{\sigma_2^2}{\sqrt{2\pi c_2^2}} \exp\left(\frac{(f - f_2)^2}{2c_2^2}\right) \tag{10}$$

The resulting ECG signal is shown in Figure 1(b), the image depicts the modulation of the QRS complex thanks to the RSA and Mayer waves. Finally, an observation uncertainty was used to the signal, this is done by adding measurement errors normally distributed with zero mean and standard deviation of $0.05mV$. With the simulation of a raw $sEMG + ECG$, the first approach can be made in the evaluation of the artifact reduction techniques, the simulated signal is shown in Figure 1(c).

The PLI interference can be modeled as a sinusoidal signal with a nominal frequency of 60 Hz (or 50 Hz depending on location). However, there are certain deviations in the nominal frequency over time, which may be due to certain instabilities in the power network, in addition to the high amplitude of the harmonic components. That is why according to[13], the PLI signal can be represented as shown in (11).

$$A_{PLI} = A\sin(2\pi f t) + B\sin(2\pi f t) \tag{11}$$

The PLI artifact is defined in the sum of a sine and cosine function. Where A and B are two second-order polynomial, $(a_0 + a_1 t + a_2 t^2)$ and $(b_0 + b_1 t + b_2 t^2)$ respectively to obtain the amplitude and frequency variations and $f$is the nominal frequency with a variation among 2 Hz[13]. The phase shift of the function was set to zero. Harmonics were added to the signal as shown in (12), according to[10].

$$A_{PLI} = \sum_{h=1}^{H} A\sin(2\pi hft) + B\sin(2\pi hft) \quad (12)$$

Where h is its harmonics. For the generation of the model, the first three harmonics were selected ($H = 3$). The PSD of the simulated clean sEMG with the simulated PLI is shown in Figure 2(a) and the simulated sEMG with ECG artifacts contaminated with PLI is shown in Figure 2(b).

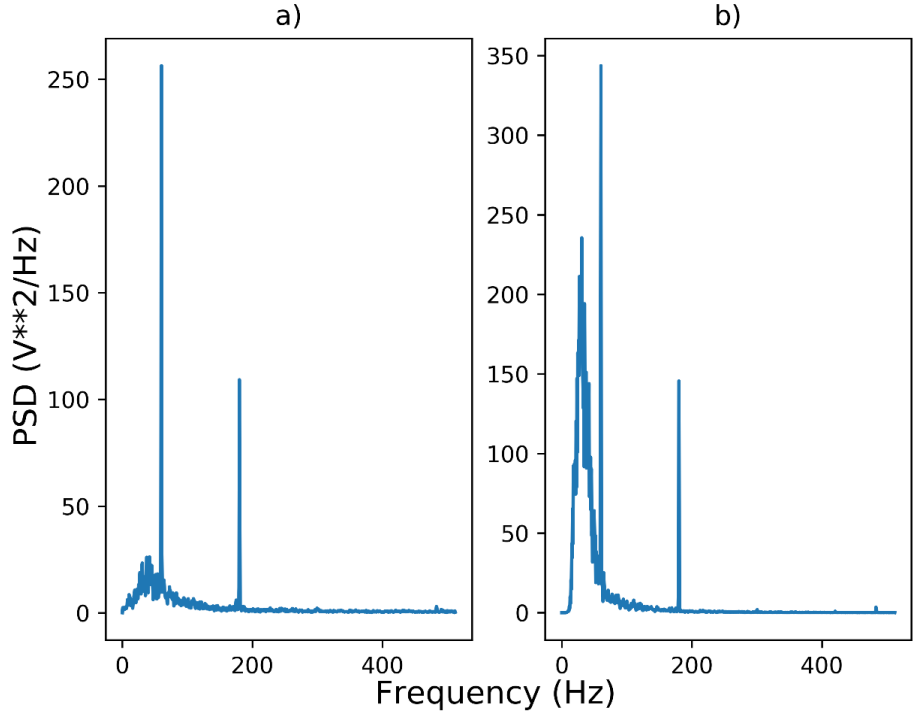

Figure 2. PSD of the simulated signal contaminated with PLI: a) clean sEMG signal contaminated with PLI; b) sEMG with ECG artifacts contaminated with PLI.

The baseline artifact can be determined as a low-frequency signal, the spectral energy of the BW signal is approximately 1 Hz. For the model that generates the BW signal, the equation (11) described previously can be used, with the difference that $f = 0$ as it is described in[13]. In this way, the expression becomes as shown in (13).

$$A_{BW} = b_0 + b_1 t + b_2 t^2 \quad (13)$$

The signal of the simulated clean sEMG with the simulated BW is shown in Figure 3(a) and the simulated sEMG with ECG artifacts contaminated with BW is shown in Figure 3(b).

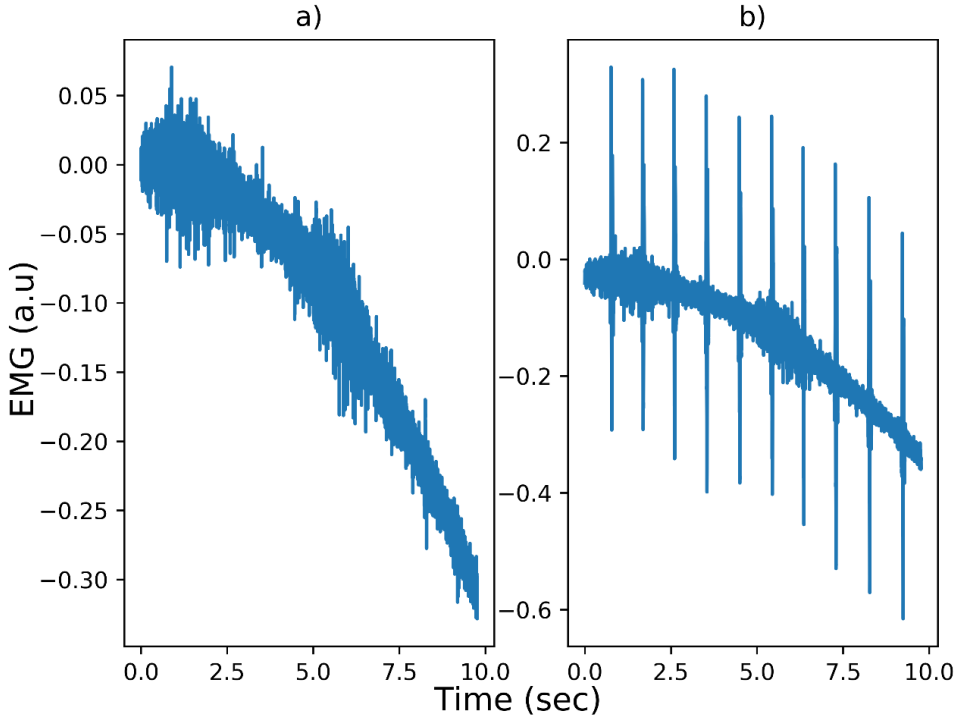

Figure 3. Simulated signal contaminated with BW: a) clean sEMG signal contaminated with BW; b) sEMG with ECG artifacts contaminated with BW.

2.2 Techniques for reduction of non-physiological interference

In this paper, 3 techniques for PLI remotion and 3 for BW remotion in sEMG signal were implemented and tested.

2.2.1 Adaptive LMS filter for PLI remotion

This corresponds to a filter class that "learns" an unknown transfer function. These types of filters use a gradient descent method in which the filter coefficients are updated based on the instantaneous error signal. This method needs a reference signal that is correlated with the noise of the signal of interest[9]. The filter is optimal by minimizing the LMS error. The structure of the filter is seen in Figure 4.

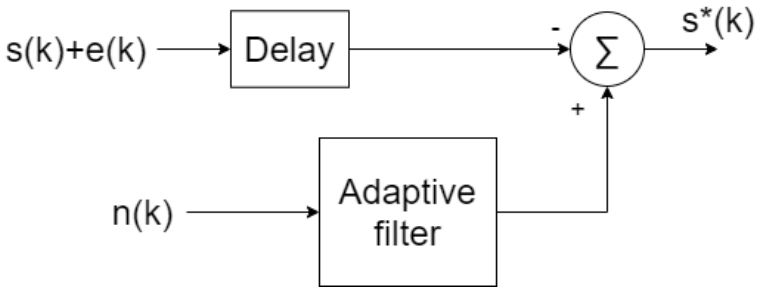

Figure 4. Structure of the removal technique of ECG from sEMG signal with a LMS filter.

Where $s(k)$is the signal of interest, $e(k)$ is the noise that contaminates the signal, $n(k)$ is the reference signal as an input of the system and $s^*(k)$ is the estimation of the signal of interest.

The coefficients of the LMS filter are determined according to (14) and the fundamental equation for the LMS filter is shown in (15).

$$H(k+1) = H(k) + 2\mu s^*(k)n(k) \quad (14)$$

$$s^*(k) = s(k) + 2\mu H^T(k)n^T(k) \quad (15)$$

Where μ is the rate of convergence and accuracy of the adaptation process and $H(k)$ is the coefficients of the adaptive filter, the finite impulse response of the adaptive filter is determined with the number of coefficients[9].

2.2.2 Spectrum interpolation technique for PLI remotion

This is a suppression method based on an interpolation in the frequency spectrum. This technique assumes that at the interference frequency (f_{PLI}) there is a peak superimposed on the signal[8]. Therefore, the actual spectral value of the signal at frequency f_{PLI} can be estimated using an interpolation. The interpolation is implemented in the result of the discrete Fourier transform (DFT) of the signal, to obtain the signal again once the spectral interpolation has been carried out, using the inverse Fourier transform. In this way, a filter is applied to the signal with a limited attenuation and not an infinite null, with this technique the information of the sEMG signal at this frequency point is assumed, instead of completely removing the information[8,10].

The technique was implemented using linear interpolation, to reduce the computational cost as much as possible. To perform the interpolation, a window (L) is defined, this window is below the value of f_{PLI} and above said value. once the two ranges of values are obtained, interpolation is implemented[8,10]. Said interpolation generates a new curve of amplitude values in the frequency values belonging to the interference. The selected window corresponds to 2 Hz and at 60 Hz, the lower value selected is 59 Hz and higher is 61 Hz.

2.2.3 EMD-based techniquefor PLI remotion

The EMD is used for the decomposition of a time-series signal into a sum of intrinsic mode functions (IMF)[6]. EMD is described in the equation.

$$s(t) = \sum_{i=1}^{N+1} c_i(t) \quad (16)$$

Where $s(t)$ is the signal decomposed and $c(t)$is the IMF and $i$is the number of IMFs from the signal.

After EMD on the sEMG signal, to identify the components that contain PLI interference, a notch filter with a band-stop frequency around 60 Hz and its harmonics is applied to each IMF, ifa_i corresponds to the filtered IMFs, the identification of the components contaminated by PLI explained in the equation (17)[6].

$$e_i = \frac{\mathrm{var}\big(c_i(t) - a_i(t)\big)}{\mathrm{var}\big(c_i(t)\big)} \quad (17)$$

Where e_i is the variable that quantifies PLI intervention in each IMF and $var[.]$ corresponds to the variance of each time series. Once the PLI intervention estimates are obtained in the signal, a threshold is implemented. If $e_i < 0.1$, then $\tilde{c_i} = c_i$; or if $e_i \geq 0.1$, then $\tilde{c_i} = a_i$. Where $\tilde{c_i}$is the processed IMFs, in other words, if the IMF is contaminated with PLI (greater than 0.1), the component with the notch filter is applied, otherwise the component is not changed.

2.2.4 High-pass filter for BW reduction

The high-pass (IIR) filter can be described as the following expression (18).

$$y(n) = \sum_{b=0}^{M} b_m x(n-m) - \sum_{m=1}^{N} a_m y(n-m) \quad (18)$$

Where b_m and a_m are the coefficients of the filter, N is the order of the filter, $x(n)$ is the input of the signal, $y(n)$ is the filtered signal. IIR filters can use a much lowerfilter order to meet the required stopband attenuation[5]. The basics topologies of the IIR filter are the Butterworth filter, Chebyshev Type I filter, Chebyshev Type II filter, and Elliptic filter. In this study, the Butterworth filter is used and with a cut-off frequency of 0.5 Hz and a filter order of 2.

2.2.5 EMD-based technique for BW reduction

To identify BW contaminated IMFs after EMD is applied, a low pass filter is used on each component with a cutoff frequency that varies as shown in 19.

$$\mathrm{f_i} = \frac{\mathrm{f_0}}{\mathrm{M^{N-i}}} \tag{19}$$

Where N is the numbers of IMFs of the signal, i is the IMF order, $f_i$is the estimated cutoff frequency of the IMF, f_0 is the cut-off frequency of $N+1$ and M is a frequency folding coefficient. In this study, f_0 and M were set to be 30and 1.15 respectively. For the identification of IMFs contaminated by BW, the equation (20) is used[6].

$$\mathrm{e_i} = \frac{\mathrm{var(d_i)}}{\mathrm{var(c_i)}} \tag{20}$$

Where e_i is the variable that quantifies BW intervention in each IMF, c_i corresponds to each IMF and d_i corresponds to each filtered IMF. Once the BW intervention estimates are obtained in the signal, a threshold is implemented. If $e_i < 0.05$, then $\tilde{b_i} = 0$; or if $e_i \varepsilon [0.05,0.5]$, then $\tilde{b_i} = d_i$; or if $e_i > 0.5$, then $\tilde{b_i} = c_i$. Where $\tilde{b_i}$ is the component processed. Once the threshold is applied to all IMFs, the denoised signal is obtained as is shown in (21).

$$\tilde{\mathrm{c_i}} = \mathrm{c_i} - \tilde{\mathrm{b_i}} \tag{21}$$

2.2.6 SSA-based technique for BW reduction

It is a technique that consists of the decomposition of a time series into a set of summable components. Each component can be interpreted as a trend, periodicity, and noise. SSA easily separates the periodicities found on different time scales, even in signals where there is a high noise content[22]. The original signal is obtained from the components only using a summation[22].

The implementation of this technique consists of several steps to decompose the signal. The first step is to transform the signal into a trajectory matrix, for this, the dimension of the window L is defined; the window size must meet the following conditions $2 \leq L \leq \frac{N}{2}$[22]. Where N is the number of data points from the time-series. The windows are formed by the subseries $\{s_i, s_{i+1} \dots, s_{i+L-1}\}$, where $i = 0,1, \dots, N-L$. By this process, each column of the matrix is determined, sliding the window over the entire signal as seen in (22).

$$\begin{aligned} \mathrm{X_0} &= (\mathrm{s_0}, \mathrm{s_1}, \dots, \mathrm{s_{L-1}})^{\mathrm{T}} \\ \mathrm{X_1} &= (\mathrm{s_1}, \mathrm{s_2}, \dots, \mathrm{s_L})^{\mathrm{T}} \\ \mathrm{X_2} &= (\mathrm{s_2}, \mathrm{s_3}, \dots, \mathrm{s_{L+1}})^{\mathrm{T}} \\ &\vdots \\ \mathrm{X_{N-L}} &= (\mathrm{s_{N-L}}, \mathrm{s_{N-L+1}}, \dots, \mathrm{s_N})^{\mathrm{T}} \end{aligned} \tag{22}$$

In this way, all the columns of the trajectory matrix (X) are created. $K = N - L + 1$ equals the number of columns that the trajectory matrix contains. This matrix is also known as a Hankel matrix. The second step is to decompose said trajectory matrix with a singular value decomposition (SVD).

$$X = U\Sigma V^{T} \tag{23}$$

Where U is a unitary matrix containing the orthonormal set of left singular vectors of X as columns and with dimensions LxL. Σ is a rectangular diagonal matrix containing L singular values of X with dimensions LxK, the singular values are $\sqrt{\lambda_i}$, where λ_i are the eigenvalues. V is a unitary matrix containing the orthonormal set of right singular vectors of X as columns with dimensions KxK[22].

The next step is to determine the elementary matrices (E_i), each of these matrices correspond to one of the components of the original signal $s(k)$. To calculate the components, an average of the antidiagonals of the given E_i is used. The components are estimated according to (24).

$$s(k) = \sum_{i=1}^{d} E(k)_i \tag{24}$$

Where d corresponds to the number of time series components of the original signal.

The last step corresponds to identify the elementary matrices (E_i) containing BW interference. For this, is proposed the same method of artifact identification shows in the EMD-based technique and described by equations 19 and 20. In this technique, f_0 and M were set to be 30 and 1.45 respectively. The threshold implemented is: if $e_i > 0.4$, then $\widetilde{E_i} = E_i - d_i$; or if $e_i \leq 0.4$ then $\widetilde{E_i} = E_i$[22].

2.3 Performance evaluation

The evaluation of the performance of the techniques in the two simulated signals is made with the following quantitative criteria: signal to noise ratio (SNR), relative error, and cross-correlation. The signal to noise ratio is calculated with equation 25.

$$SNR = 10\log_{10}\frac{var(s(k))}{var(s(k) - s^{*}(k))} \tag{25}$$

Where the variance of $s(k)$ is the variance of the simulated sEMG signal (Figure 1(c)) and the variance of $s^{*}(k)$ is the estimated sEMG signal by the techniques of PLI and BW artifact removal. The higher the value of this measure, the better the performance of the technique [23].

The relative error (RE) is estimated using the following equation (26).

$$RE = \frac{\sum(S(f) - S^{*}(f))^2}{\sum(S(f))^2} \tag{26}$$

Where, $S(f)$ and $S^{*}(f)$are the spectral density of the simulated sEMG signal and the estimated sEMG signal by the techniques of PLI and BW artifact removal, respectively. The lower value of this measure indicates the technique with the best performance [23].

The cross-correlation (CC) is calculated with (27).

$$CC = \left(\frac{\sum s(k)s_{*}(k)}{(\sum s(k))^2(\sum s^{*}(k))^2}\right) \tag{27}$$

The increase of the cross-correlation indicates a better performance of the technique. Coherence was estimated between the original sEMG and the processed signal, this indicator provides a measure of the performance in the frequency domain. A higher coherence value indicates a better performance of the technique. The equation for the coherence is (28).

$$\mathrm{Coh(f)} = \frac{\left|\mathrm{P_{s(n)s^*(n)}(f)}\right|^2}{\mathrm{P_{s(n)}(f)P_{s^*(n)}(f)}} \tag{28}$$

Where, $P_{s(n)s^*(n)}(f)$is the cross-spectral density between the simulated sEMG and the processed sEMG signal, and the $P_{s(n)}(f)$and $P_{s^*(n)}(f)$their respective auto-spectra.

2.4 Tests in online and automatic implementation

The performance of each of the techniques was estimated in a real-time record. To identify the most suitable techniques for online implementations, during the registration a time window was defined where the techniques were applied, a window that changes every 10 seconds. The selected time windows were 10, 5, 2, 1, 0.5, and 0.3 seconds. In each of these time windows, the computational cost was determined. This process was done on specific hardware and the performance of each technique was also evaluated with each amount of data.

3. RESULTS

Each of the three PLI removal techniques was implemented in the simulated signals of clean sEMG and contaminated by ECG, as observed in Figure 5, a PSD analysis of the result of each technique compared to the original signal.

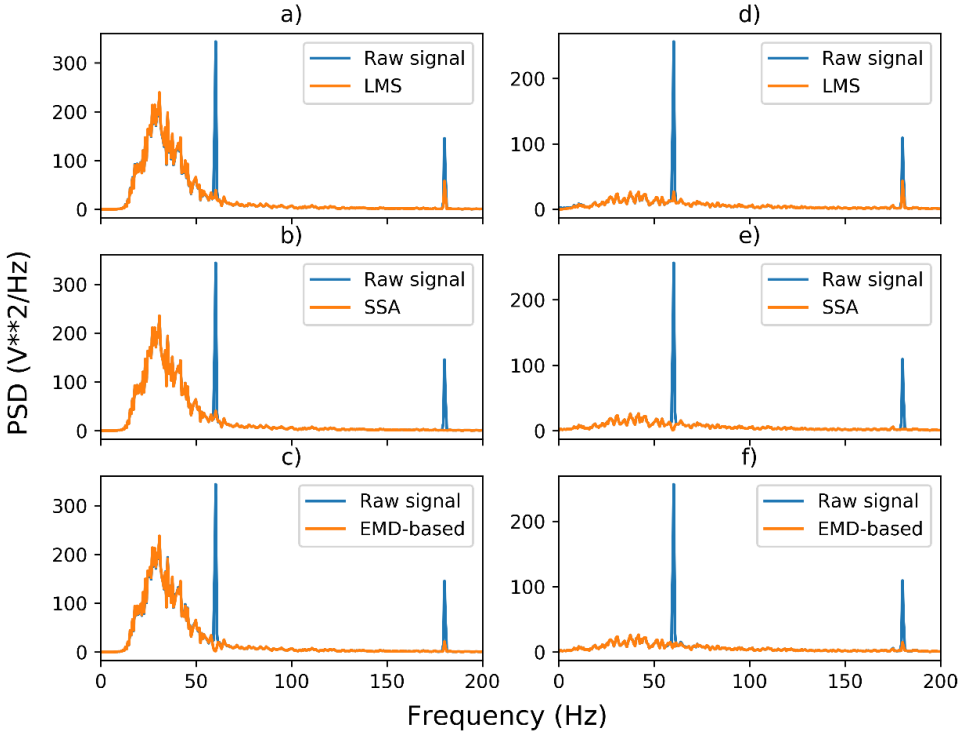

Figure 5. PSD resulted of each technique compared with PSD of the original signal, where: a) corresponds to the adaptive LMS filter applied to the sEMG+ECG signal; b) corresponds to the spectrum interpolation technique applied to the sEMG+ECG signal; c) corresponds to the EMD-based technique applied to the sEMG+ECG signal; d) corresponds to the adaptive LMS filter applied to the clean sEMG signal; d) corresponds to the spectrum interpolation technique applied to the clean sEMG signal and e) corresponds to the EMD-based technique applied to the pure sEMG signal.

The adaptive LMS filter is applied with an order of 2 and a step size of 5 for the two modeled signals. The reference signal was generated by adding two cosine functions, one with a frequency of 60 Hz and the other with 180 Hz, according to the interference of PLI and its simulated harmonics in the

signals.

The result of the adaptive LMS filter technique is seen in Figure 5(a) for the sEMG signal contaminated with ECG and in Figure 5(d) for the clean sEMG signal.

With the spectrum interpolation technique, a frequency window between 59 Hz to 61 Hz and 179 to 181 Hz was separated in each of the components. Then in every range, a linear interpolation was performed, taking as initial data, the same window below 59 and above 61, the same procedure in the 180 Hz component. The result of this technique is seen in Figure 5(b) for the sEMG signal contaminated with ECG and in Figure 5(e) for the clean sEMG signal.

For the EMD-based technique, the signal was decomposed into 12 IMFs, from which the threshold was filtered and applied in the 60 and 180 Hz components. The results of the EMD-based technique are seen in Figure 5(c) for the sEMG signal contaminated with ECG and in Figure 5(f) for the clean sEMG signal.

To the results of the different techniques SNR, RE, and CC values were estimated to evaluate the performance of each technique in the two types of modeled signals. The values of these criteria are shown in Table 1 for the clean sEMG model and the model of sEMG contaminated with ECG.

Table 1. Comparison of the quantitative criteria of every artifact removal technique for sEMG simulated signal and sEMG + ECG simulated signal.

sEMG simulated signal			
Criteria	Adaptive LMS filter	Spectrum interpolation technique	EMD-based technique
SNR	0.1001	0.3396	0.1821
RE	0.0723	0.0312	0.0714
CC	0.0631	0.0661	0.0642
sEMG+ECG simulated signal			
Criteria	Adaptive LMS filter	Spectrum interpolation technique	EMD-based technique
SNR	0.1729	0.0897	0.0562
RE	0.0438	0.0264	0.0198
CC	0.0165	0.0169	0.0169

The spectral coherence between the original signal and the signal processed by the artifact removal techniques is observed in Figure 6, for both the clean sEMG signal and the sEMG signal contaminated with ECG.

The signal is decomposed into 12 IMFs with the EMD-based technique, the filters have the following values for cutoff frequencies: [3.6868, 4.2398, 4.8758, 5.6072, 6.4482, 7.4155, 8.5278, 9.8070, …… 11.2781, 12.9698, 14.9153, 17.1525, 19.7254, 22.6843] Once the threshold has been implemented for each simulated signal, the results of the PSD are shown in Figure 7(b) for the sEMG with ECG artifacts and Figure 7(e) for clean sEMG.

For the SSA-based technique, the signal was decomposed into 12 components, the values of cutoff frequencies of the filter are: [0.2395, 0.3473, 0.5035, 0.7301, 1.0587, 1.5352, 2.2261, 3.2278, 4.6803, ….. 6.7865, 9.8405, 14.2687] Once the threshold has been implemented for each simulated signal, the results of the PSD are shown in Figure 7(c) for the sEMG with ECG artifacts and Figure 7(d) for clean sEMG.

Regarding the BW removal techniques, the same implementation as previously described was made, Figure 7 shows the comparison of the PSD of the original signal, that is, the models of pure sEMG and sEMG contaminated with ECG, with the processed signals for each of the techniques.

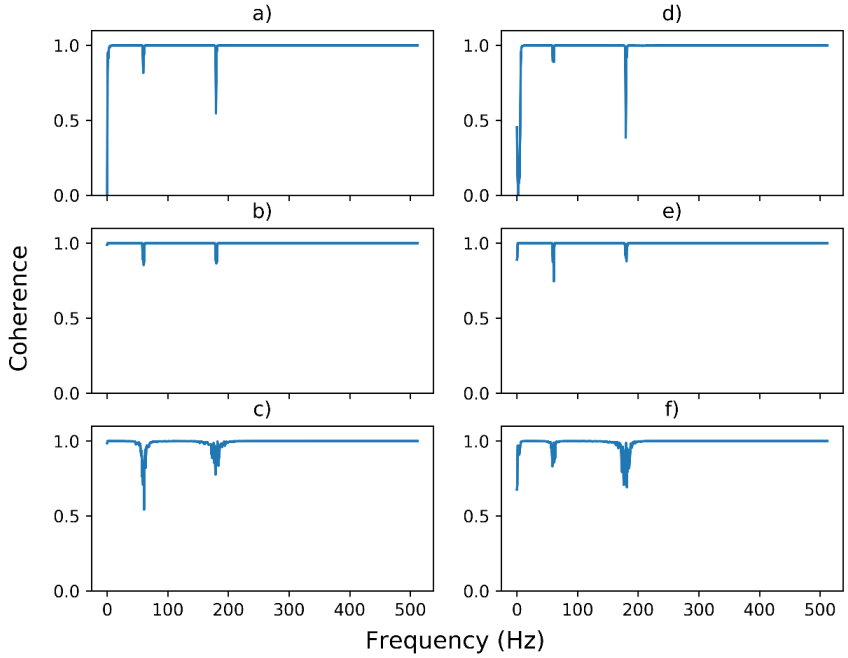

Figure 6. Spectral coherence of the signals processed by the artifact removal techniques with the original signal: a) corresponds to the adaptive LMS filter applied to the sEMG+ECG signal; b) corresponds to the spectrum interpolation technique applied to the sEMG+ECG signal; c) corresponds to the EMD-based technique applied to the sEMG+ECG signal; d) corresponds to the adaptive LMS filter applied to the clean sEMG signal; d) corresponds to the spectrum interpolation technique applied to the clean sEMG signal and e) corresponds to the EMD-based technique applied to the clean sEMG signal.

Furthermore, the results of SNR, CC, and RE were estimated for each technique, both in the modeled signal of the clean sEMG and in the modeled signal of sEMG contaminated with ECG (Table 2). Finally, the spectral coherence of each of the techniques with the original signals was estimated, as observed in Figure 8.

Once each of the processed signals corresponding to the techniques of BW and PLI removal applied to both the models and the recorded sEMG has been obtained and the criteria for performance evaluation has been calculated, the computational cost of each of the techniques is estimated to determine which techniques for BW removal and PLI removal are the most suitable in online and automatic applications. The removal techniques were compiled on hardware which is a small single-board computer known as Raspberry Pi to verify its operation in automatic applications in independent hardware systems of a computer and to be able to estimate the latency between the original and the estimated signal when the processing is done in limited hardware.

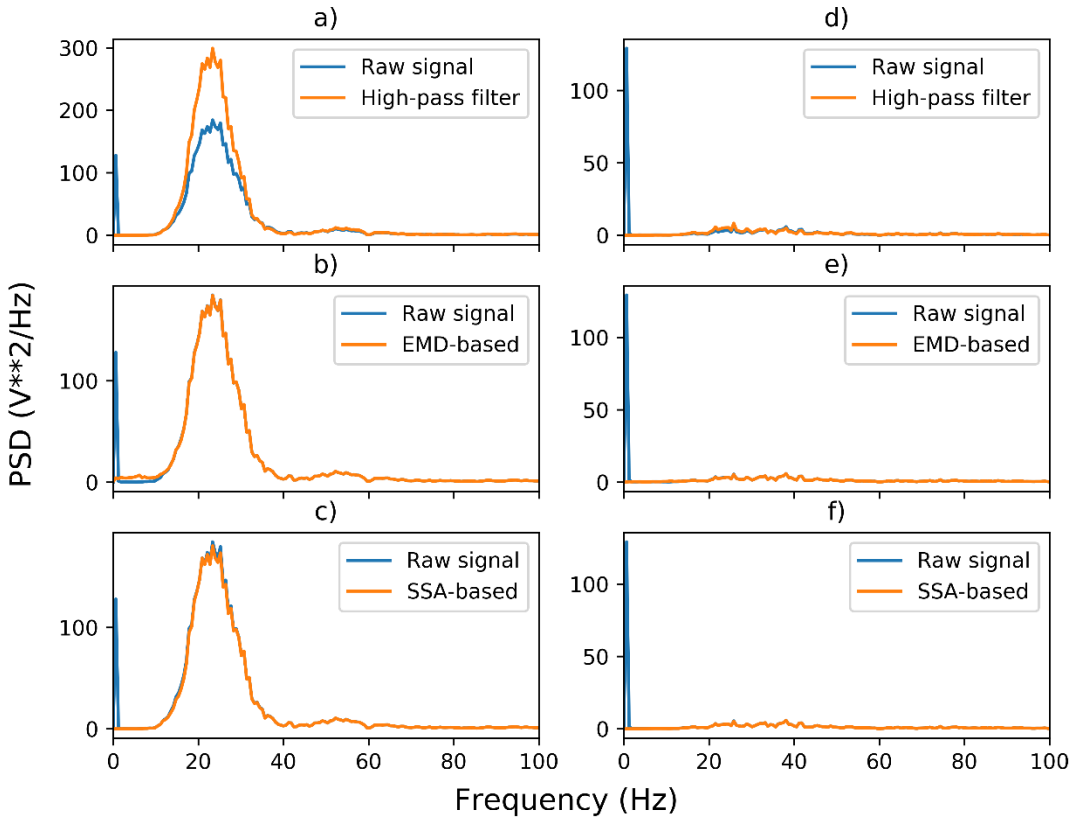

Figure 7. PSD resulted of each technique compared with PSD of the original signal, where: a) corresponds to theIIR High-Pass Filterapplied to the sEMG+ECG signal; b) corresponds to the EMD-based technique applied to the sEMG+ECG signal; c) corresponds to the SSA-based technique applied to the sEMG+ECG signal; d) corresponds to the IIR High-Pass Filterapplied to the clean sEMG signal; d) corresponds to the EMD-based technique applied to the clean sEMG signal and e) corresponds to the SSA-based technique applied to the clean sEMG signal.

The specifications of the small single-board are a Broadcom BCM2837B0, Cortex-A53 (ARMv8) 64-bit SoC @ 1.4GHz processor, 1GB RAM, and 32GB storage memory. The operating system implemented on the small single-board is the Raspbian version from 2019-04-08 and the techniques were developed and compiled in Python 3.5.6. Each of the techniques was implemented in different time windows in modeled signals that contain BW and PLI artifacts. The time windows were 10, 5, 2, 1, 0.5, and 0.3 seconds. Each window was tested in a length of time of ten seconds and the estimated compile-time across the window is averaged.

Table 2. Comparison of the quantitative criteria of every artifact removal technique for sEMG model and sEMG+ECG simulated signal.

sEMG simulated signal			
Criteria	IIR High-Pass Filter	EMD-based technique	SSA-based technique
SNR	0.5276	0.5025	0.5621
RE	0.1145	0.1457	0.1117
CC	0.4974	0.4873	0.5002

sEMG+ECG simulated signal			
Criteria	IIR High-Pass Filter	EMD-based technique	SSA-based technique
SNR	0.1005	0.0077	1.5940
RE	0.2995	0.3091	0.2989
CC	0.0317	0.0311	0.0319

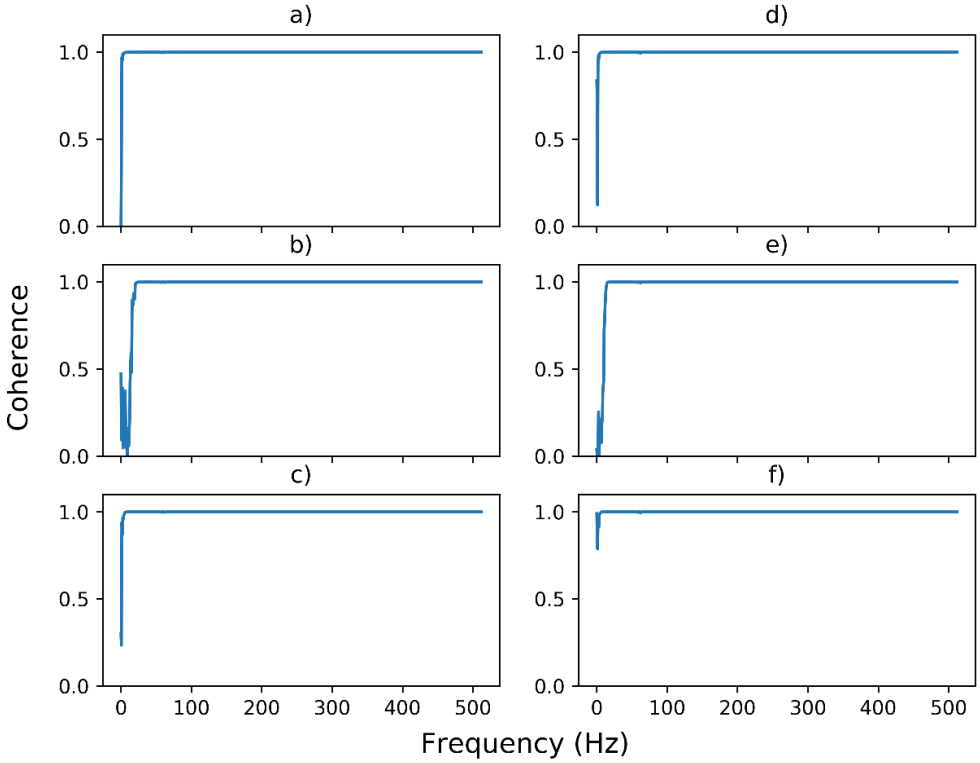

Figure 8. Spectral coherence of the signals processed by the artifact removal techniques with the original signal:a) corresponds to the IIR High-Pass Filterapplied to the sEMG+ECG signal; b) corresponds to the EMD-based technique applied to the sEMG+ECG signal; c) corresponds to the SSA-based technique applied to the sEMG+ECG signal; d) corresponds to the IIR High-Pass Filterapplied to the clean sEMG signal; d) corresponds to the EMD-based technique applied to the clean sEMG signal and e) corresponds to the SSA-based technique applied to the clean sEMG signal.

Table 3. Mean runtime of every BW removal and PLI techniques in different time windows.

BW removal technique			
Window (seconds)	IIR High-Pass Filter (seconds)	EMD-based technique (seconds)	SSA-based technique (seconds)
0.3	0.0293	0.1438	0.0144
0.5	0.0501	0.4567	0.5819
1	0.1058	0.9623	0.1087

5	0.5273	3.4452	1.5478
10	1.1020	6.6726	7.1894

PLI removal technique			
Window (seconds)	LMS filter (seconds)	Spectrum interpolation (seconds)	EMD-based technique (seconds)
0.3	0.0237	2.9458	0.4037
0.5	0.0351	2.9436	1.3222
1	0.0626	3.0206	2.1879
5	0.2874	3.3231	7.1894
10	0.5667	4.0062	11.1071

It should be noted that in the tests where the execution time of each of the techniques was measured for both the removal of PLI and BW, although these results vary due to various factors, the type of hardware, compiler, programming language, optimization code, among others. The implementation of these tests seeksto find the techniques that have the best performance with the least delay difference between the signal processed and the one acquired in real-time.

4. DISCUSS

In this paper, 3 artifact removal techniques for PLI and 3 for BW were implemented according to literature reports [4,5,7–9,16]. With the selected techniques, the performance in removing the artifacts without distorting the frequency components corresponding to the signal and the computational cost.

In the two simulated sEMG signals with PLI, the three removal techniques were implemented. According to results in the frequency domain, the adaptive LMS filter in the two simulated signals, a considerable attenuation is observed in the peak located approximately at the 60 Hz frequency. This result is observed for both, for the pure sEMG signal and the contaminated with ECG. However, in the two signals a remnant located in the harmonic corresponding to a frequency of 180 Hz is also observed, where although a smaller amplitude, the peak is maintained. However, in the two signals, a remnant located in the harmonic corresponding to a frequency of 180 Hz is also observed, where the peak is maintained although with a smaller amplitude. The result of this technique may be due to the reference signal, said signal is constructed by a sinusoidal function with the frequency values corresponding to the PLI, which is at 60 Hz and its harmonics. However, it should be noted that the amplitude of the PLI is variable according to conditions such as the state of the electrical network, the electrodes of the acquisition device, the circuits of the acquisition device, among others. The change that said magnitude has in the signal interference is, without a doubt, a limitation of this technique, since, as observed in Figure 5(a) and Figure 5(d), it does not completely attenuate the artifact if it presents a greater magnitude in that frequency component.

The results of the spectral interpolation technique shown a better result than the previous technique. According to Figure 5(b) and Figure 5(e), the amplitude peaks corresponding to the PLI artifacts are completely attenuated and the resulting amplitude is consistent with the frequency activity of the signal. It should be noted that this technique is an estimate of the real value of the signal, that is, the frequency values corresponding to the artifacts are replaced by the calculated value of a linear interpolation of the signal. The resulting information on these frequency components is determined as

a mathematical approximation of the actual signal.

In the EMD-based technique, according to Figure 5(c) and Figure 5(f), a complete attenuation is presented in the 60 Hz component; however, in the 180 Hz harmonic, a remnant remained, but of less amplitude compared to the adaptive LMS filter technique. From inspection of the PSD, the spectral interpolation technique is the one that presents the best result, followed by the EMD-based technique.

From Table 1, the results obtained from each of the estimated values for each criterion can be analyzed. Regarding the results obtained from the SNR, the technique with the best result for the two simulated signals is the spectral interpolation with a higher value compared to the other two techniques; in RE in the clean sEMG signal, the technique with the least relative error is the spectral interpolation technique and in the sEMG signal contaminated with ECG, the EMD-based technique has a slightly smaller relative error than the spectral interpolation technique; and as for the CC, the three techniques presented very similar values in the two signals, the spectral interpolation technique being slightly higher in the pure sEMG signal and the SEMG signal contaminated with ECG, the spectral interpolation technique and the base-EMD have the same value. The coherence Figure 6 confirms the spectral interpolation as the best technique, being the one that shows the smallest difference between the original and the filtered signal between the 60 and 180 Hz components.

In BW removal, the first technique implemented is the IIR High-Pass Filter. In Figure 7(a) and Figure 7(d), removal of the amplitude peaks corresponding to the artifact is observed. However, in the sEMG signal contaminated with ECG, a greater amplitude occurs, this amplitude offset can be considered as a distortion of the original signal, which is not suitable.

In the EMD-based technique, according to Figure 7(b) and Figure 7(e), the artifact corresponding to BW is correctly attenuated and the rest of the signal frequency activity is not distorted or modified in terms of phase, frequency, or amplitude.

Finally, for the SSA-based technique, according to Figure 7(c) and Figure 7(f), the artifact corresponding to BW is correctly attenuated and the rest of the signal frequency activity is not distorted, except for some maximum amplitude values in the ECG contaminated signal.

When evaluating the values obtained for each criterion in Table 2 the SSA-based technique obtains the best SNR value, being the highest compared to the other two techniques in the two signals; the RE of lesser value in the two signals corresponds to the SSA-based technique, and the highest value CC also corresponds to the SSA-based technique. The estimated values in each criterion inferred SSA-based as the best technique and the visual inspection of the PSD (Figure 7) shows that it attenuates the artifacts corresponding to BW that are found in the lower frequency components and that it does not significantly distort the signal compared to the original signal. Figure 8 corresponding to the coherence values confirms the SSA-based technique as the best since it is the one that shows the least difference with the original signal in the lower frequency components.

In Table 3 the runtime is shown for the removal PLI techniques, the least computational cost technique for the removal of PLI is the adaptive LMS filter, while the spectral interpolation technique, although it is the one with the best performance, has a high computational cost. The EMD-based technique has a high computational cost in signals of a large amount of data, but as the number of data is reduced, the compilation times are considerably reduced. For BW removal technique, it can be seen in Table 3 that the least computational cost technique in the 10-second window is the moving average filter; however, by reducing the window, the SSA-based technique reduces the runtime significantly, so that in the 0.5 second window it has a runtime similar to the moving average filter technique and in the 0.3 second window it has a shorter runtime than the moving average technique.

5. CONCLUSIONS

In this study, several BW and PLI removal techniques in sEMG signals were selected according to a bibliographic review. The selected techniques were evaluated on sEMG signals from the respiratory muscle diaphragm and it was determined how suitable they were for applications such as monitoring in ventilator-supported patients or other clinical applications. During the evaluation of these techniques, it was verified that they fulfilled conditions such as the performance in removing the BW and PLI artifacts. Thus, for PLI removal techniques, the spectral interpolation technique, for online applications, does not seem to be suitable despite the good performance is shown, this due to its computational cost, the same problem is presented by the EMD-based technique, the adaptive LMS filter has a low computational cost but it presents problems in terms of its reference signal that can affect its performance when removing artifacts, however, in the real sEMG record, it presented a very good performance. For the spectral interpolation technique, its implementation should be optimized to reduce compilation time and may be suitable for online applications. Finally, for the BW removal techniques, the SSA-based technique proved to be the best performing and its computational cost is considerably reduced in small time windows, which makes it ideal to implement in this type of time windows. On the other hand, the EMD-based technique presented a high computational cost, unlike the IIR High-Pass Filter, although in a frequency analysis and criteria estimates, it turned out to be the one with the lowest performance.

REFERENCES

[1] De Luca C J, Donald Gilmore L, Kuznetsov M and Roy S H 2010 Filtering the surface EMG signal: Movement artifact and baseline noise contamination *J. Biomech.*
[2] Saadeh P B, Crisafulli C F, Sosner J and Wolf E 1993 Needle electromyography of the diaphragm: A new technique *Muscle Nerve*
[3] Gilliatt R W 1962 Electrodiagnosis and electromyography in clinical practice *Br. Med. J.*
[4] Salazar Sánchez M B, Hernández Valdivieso A M and Mañanas Villanueva M Á 2017 Assessment of mechanically ventilated patients intoxicated with organophosphates by a novel surface electromyographic index *J. Crit. Care*
[5] An X and Stylios G K 2020 Comparison of motion artefact reduction methods and the implementation of adaptive motion artefact reduction in wearable electrocardiogram monitoring *Sensors (Switzerland)*
[6] Zhang X and Zhou P 2013 Filtering of surface EMG using ensemble empirical mode decomposition *Med. Eng. Phys.*
[7] Ladrova M, Martinek R, Nedoma J and Fajkus M 2019 Methods of power line interference elimination in EMG signals *J. Biomimetics, Biomater. Biomed. Eng.*
[8] Mewett D T, Reynolds K J and Nazeran H 2004 Reducing power line interference in digitised electromyogram recordings by spectrum interpolation *Med. Biol. Eng. Comput*.
[9] Yacoub S and Raoof K 2008 Noise Removal from Surface Respiratory EMG Signal Int. *J. Electron. Commun. Eng.*
[10] Soedirdjo S D H, Ullah K and Merletti R 2015 Power line interference attenuation in multi-channel sEMG signals: Algorithms and analysis *Proceedings of the Annual International Conference of the IEEE Engineering in Medicine and Biology Society, EMBS*
[11] Yadav J, Singh A and Kumar M 2012 Comparative study of various techniques for elimination of noise in EMG signal Int. *J. Sci. Eng. Res.*
[12] Bhateja V, Srivastava A, Tiwari D K, Anand D, Satapathy S C, Nhu N G and Le D N 2018 Baseline correction in EMG signals using mathematical morphology and canonical correlation analysis *Advances in Intelligent Systems and Computing*
[13] Zivanovic M and González-Izal M 2013 Simultaneous powerline interference and baseline wander removal from ECG and EMG signals by sinusoidal modeling *Med. Eng. Phys.*
[14] Zhan C, Yeung L F and Yang Z 2010 A wavelet-based adaptive filter for removing ECG interference in EMGdi signals *J. Electromyogr. Kinesiol*.

[15] Willigenburg N W, Daffertshofer A, Kingma I and van Dieën J H 2012 Removing ECG contamination from EMG recordings: A comparison of ICA-based and other filtering procedures *J. Electromyogr. Kinesiol.*
[16] Van Vugt J P P and Van Dijk J G 2001 A convenient method to reduce crosstalk in surface EMG *Clin. Neurophysiol.*
[17] Williams E E, Hunt K A, Jeyakara J, Subba-Rao R, Dassios T and Greenough A 2020 Electrical activity of the diaphragm following a loading dose of caffeine citrate in ventilated preterm infants *Pediatr. Res.*
[18] Bellani G, Bronco A, Arrigoni Marocco S, Pozzi M, Sala V, Eronia N, Villa G, Foti G, Tagliabue G, Eger M and Pesenti A 2018 Measurement of diaphragmatic electrical activity by surface electromyography in intubated subjects and its relationship with inspiratory effort *Respir. Care*
[19] Sarlabous L, Estrada L, Cerezo-Hernández A, Sietske S V., Torres A, Jané R, Duiverman M and Garde A 2019 Electromyography-based respiratory onset detection in copd patients on non-invasive mechanical ventilation *Entropy*
[20] Sánchez M B S, Valdivieso A M H, Villanueva M Á M and Salazar A F Z 2017 Potential clinical application of surface electromyography as indicator of neuromuscular recovery during weaning tests after organophosphate poisoning *Rev. Bras. Ter. Intensiva*
[21] Sörnmo L and Laguna P 2005 The Electrocardiogram—A Brief Background Bioelectrical Signal Processing in Cardiac and Neurological Applications
[22] Maddirala A K and Shaik R A 2016 Motion artifact removal from single channel electroencephalogram signals using singular spectrum analysis *Biomed. Signal Process. Control*
[23] Deng Y, Wolf W, Schnell R and Appel U 2000 New aspects to event-synchronous cancellation of ECG interference: An application of the method in diaphragmatic EMG signals *IEEE Trans. Biomed. Eng.*
[24] Hashemi S E, Ali Ahmadi-Pajouh M and Shamsi E 2018 Modeling and Simulation of EMG Signal and H-Reflex in Healthy Human Subject 2018 *25th Iranian Conference on Biomedical Engineering and 2018 3rd International Iranian Conference on Biomedical Engineering, ICBME 2018*
[25] McSharry P E, Clifford G D, Tarassenko L and Smith L A 2003 A dynamical model for generating synthetic electrocardiogram signals *IEEE Trans. Biomed. Eng.*
[26] Malik M 1996 Task Force of The European Society of Cardiology and The North American Society of Pacing and Electrophysiology *Eur. Heart J.*
[27] McSharry P E, Clifford G, Tarassenko L and Smith L A 2002 Method for generating an artificial RR tachogram of a typical healthy human over 24-hours *Computers in Cardiology*